remote sensing

MDPI

Article

Benchmarking Under- and Above-Canopy Laser Scanning Solutions for Deriving Stem Curve and Volume in Easy and Difficult Boreal Forest Conditions

Jesse Muhojoki [1,*,†], Daniella Tavi [1,†], Eric Hyyppä [1], Matti Lehtomäki [1], Tamás Faitli [1], Harri Kaartinen [1], Antero Kukko [1,2], Teemu Hakala [1] and Juha Hyyppä [1,2]

[1] Department of Remote Sensing and Photogrammetry, Finnish Geospatial Research Institute FGI, The National Land Survey of Finland, Vuorimiehentie 5, FI-02150 Espoo, Finland; daniella.tavi@nls.fi (D.T.); eric.hyyppa@nls.fi (E.H.); matti.lehtomaki@nls.fi (M.L.); tamas.faitli@nls.fi (T.F.); harri.kaartinen@nls.fi (H.K.); antero.kukko@nls.fi (A.K.); teemu.hakala@nls.fi (T.H.); juha.hyyppa@nls.fi (J.H.)

[2] Department of Built Environment, School of Engineering, Aalto University, P.O. Box 11000, FI-00076 Aalto, Finland

* Correspondence: jesse.muhojoki@nls.fi

† These authors contributed equally to this work.

Abstract: The use of mobile laser scanning for mapping forests has scarcely been studied in difficult forest conditions. In this paper, we compare the accuracy of retrieving tree attributes, particularly diameter at breast height (DBH), stem curve, stem volume, and tree height, using six different laser scanning systems in a managed natural boreal forest. These compared systems operated both under the forest canopy on handheld and unmanned aerial vehicle (UAV) platforms and above the canopy from a helicopter. The complexity of the studied forest sites ranged from easy to difficult, and thus, this is the first study to compare the performance of several laser scanning systems for the direct measurement of stem curve in difficult forest conditions. To automatically detect tree stems and to calculate their attributes, we utilized our previously developed algorithm integrated with a novel bias compensation method to reduce the overestimation of stem diameter arising from finite laser beam divergence. The bias compensation method reduced the absolute value of the diameter bias by 55–99%. The most accurate laser scanning systems were equipped with a Velodyne VLP-16 sensor, which has a relatively low beam divergence, on a handheld or UAV platform. In easy plots, these systems found a root-mean-square error (RMSE) of below 10% for DBH and stem curve estimates and approximately 10% for stem volume. With the handheld system in difficult plots, the DBH and stem curve estimates had an RMSE under 10%, and the stem volume RMSE was below 20%. Even though bias compensation reduced the difference in bias and RMSE between laser scanners with high and low beam divergence, the RMSE remained higher for systems with a high beam divergence. The airborne laser scanner operating above the forest canopy provided tree attribute estimates close to the accuracy of the under-canopy laser scanners, but with a significantly lower completeness rate for stem detection, especially in difficult forest conditions.

Keywords: airborne laser scanning; mobile laser scanning; individual tree detection; stem curve; point cloud processing; boreal forest

Citation: Muhojoki, J.; Tavi, D.; Hyyppä, E.; Lehtomäki, M.; Faitli, T.; Kaartinen, H.; Kukko, A.; Hakala, T.; Hyyppä, J. Benchmarking Under- and Above-Canopy Laser Scanning Solutions for Deriving Stem Curve and Volume in Easy and Difficult Boreal Forest Conditions. *Remote Sens.* **2024**, *16*, 1721. https://doi.org/10.3390/rs16101721

Academic Editors: Henning Buddenbaum and Krzysztof Stereńczak

Received: 3 April 2024
Revised: 4 May 2024
Accepted: 10 May 2024
Published: 13 May 2024

1. Introduction

Forest inventories typically utilize reference measurements of individual trees measured in the field as well as remote sensing data covering large forest areas to provide detailed knowledge about forests. The importance of this knowledge lies in the wide-ranging ecosystem services that forests offer, which include environmental services such as climate change mitigation, economic benefits such as timber and biofuel, as well as cultural and recreational amenities [1]. The demand for accurate tree reference measurements is also

growing, driven by an increasing need for multi-functional forestry and the needs of industries such as logging, forest management, and conservation [1]. In this context, the speed of reference data collection and the related accuracy of the derived tree attributes emerge as important factors in obtaining automatic field reference measurements of individual trees.

Reference data collection has traditionally been a manual process using equipment such as tape measures, calipers, and clinometers [2,3]. However, due to the prohibitively slow speed of this process, substantial research effort has been put into alternative and potentially automatic methods in the past few decades. The most widely studied method is laser scanning, which includes stationary terrestrial laser scanning (TLS), under-canopy mobile laser scanning (MLS), and above-canopy airborne laser scanning (ALS). In this paper, we use the term kinematic laser scanning to cover both MLS and ALS. Note that unmanned aerial vehicle (UAV, drone) laser scanning can be either MLS or ALS, depending on whether the drone operates above or under the canopy. Laser scanning methods can measure the key attributes of individual trees, such as diameter at breast height (DBH) and its extension stem curve, i.e., diameter as a function of height, as well as stem volume, location, species, and tree height, up to several magnitudes faster than manual methods. In addition to the slow collection speed that hinders manual data collection, the accuracy of manually collected tree measurements varies and the height of tall trees is often overestimated [4]. As a further benefit of laser scanning methods, they provide non-destructive and automatic measurements of tree attributes for visible trees [5–7]. In contrast, the most accurate manual method for obtaining the stem curve involves using a logging machine to cut down a tree [6]. In addition, the laser scanning-derived stem curves can be used alongside tree height to estimate stem volume [7–11], which may provide a more accurate estimate of the stem volume compared to national allometric models that have traditionally been used [7]. Thus, laser scanning approaches can offer a more time-efficient way of gathering field reference measurements compared to manual methods, provided that the measurements are accurate enough for operational use. The required accuracy is suggested to be 10% for stem volume estimates [12].

Section 2.1 outlines the ample research that has been conducted on different laser scanning methods in collecting individual tree measurements. Some of these studies have compared laser scanning methods for reference data collection in forests. For instance, various studies have specifically compared an individual TLS and MLS system [13–16]. Oveland et al. [17] and Liang et al. [18] have also studied TLS alongside two different MLS systems. Moreover, Chudá et al. [19] compared two MLS systems. Meanwhile, there have been fewer research studies offering more comprehensive comparisons across different types of laser scanning methods and systems. One notable example of a larger-scale comparison is the study by Hyyppä et al. [8], where various ground-based MLS systems as well as under- and above-canopy UAV laser scanning systems were evaluated. However, new sensor solutions have appeared since then with different divergences and beam sizes. Additionally, there has been an absence of comparisons of automatic stem curve extraction by different laser scanning systems and limited research overall comparing the performance of different systems in difficult forest conditions containing 1000–2000 trees/ha.

In this study, we compare the accuracy of the tree attribute acquisition of several kinematic, state-of-the-art laser scanning systems in a boreal forest. The systems include both commercially available and in-house-developed systems, operating under and above the forest canopy. Furthermore, the systems studied in this work also include the autonomous under-canopy drone systems of Hovermap (Emesent, Milton, Australia) and Deep Forestry (Deep Forestry, Uppsala, Sweden). In total, we compare six kinematic laser scanning systems in six test sites with varying complexities, including difficult forest stands with varied tree species compositions. We utilize an automatic stem extraction method to calculate the tree attributes for each individual tree and compare the results to reference measurements acquired through the combination of stem curves derived from highly accurate TLS data and tree heights estimated from high-density ALS data. This study is a continuation of Tavi [20], where these laser scanning systems were compared in terms of their tree attribute

estimation accuracy. As an addition, we propose a bias compensation method in order to reduce the overestimation of the stem curve caused by the relatively wide laser beams of kinematic laser scanners. Therefore, the objectives of this study are to compare the completeness and correctness of stem detection between these kinematic laser scanning systems as well as to compare the accuracy of the DBH, stem curve, tree height, and stem volume estimation. In addition, we evaluate the effectiveness of the bias compensation method and whether this calibration generalizes to plots with vastly different tree composition and density compared to the plot used for calibration. As some of the systems have the same or similar hardware, we can also compare the influence of software-based positioning solutions on the results. An overview of this paper is presented in Figure 1.

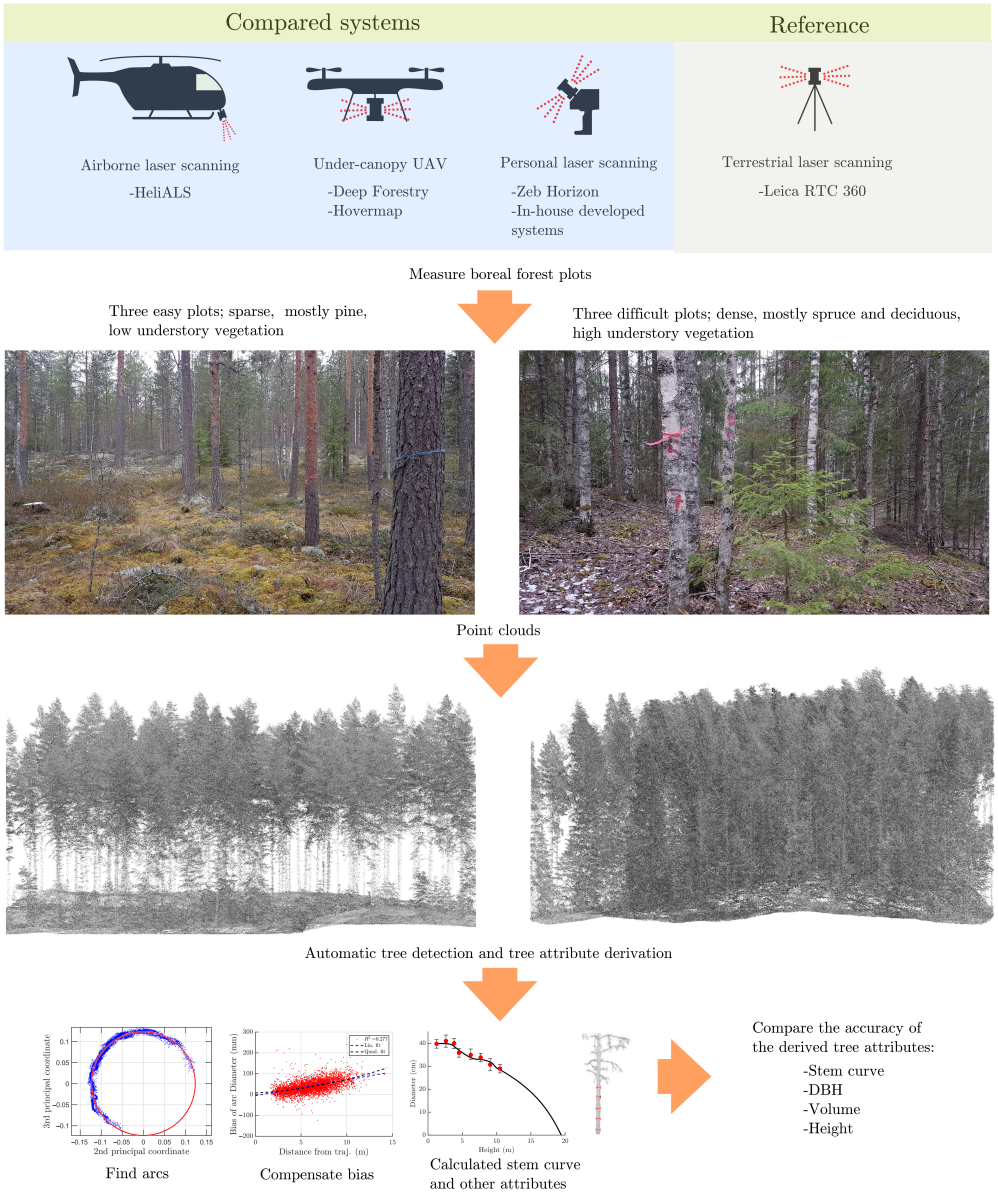

Figure 1. Overview and workflow for the comparison of laser scanning systems. The top row illustrates the compared systems together with the TLS system used to acquire the reference for stem curve. Representative photographs of *easy* and *difficult* plots are shown in the second row, followed by an illustration of the resulting point clouds in the third row. Tree attributes are automatically derived from the point clouds.

2. Material and Methods

2.1. Related Work

This section summarizes the prior work related to the different laser scanning methods and their ability to obtain tree attribute measurements. One of these methods is under-canopy MLS, which is a kinematic laser scanning approach that covers both UAV laser scanning as well as other ground-based MLS techniques. Simultaneous localization and mapping (SLAM) has been incorporated into under-canopy systems as a way to reduce positioning errors that result from the weak Global Navigation Satellite System (GNSS) signal under the forest canopy [21–24] or even to operate without a GNSS receiver [13,16,19,25,26]. These under-canopy MLS methods have been found to detect trees with a high success rate, with some studies showing the completeness of stem detection reaching above 90% [13,15,16,27,28]. Similarly high detection rates of over 90% have been found with under-canopy UAV laser scanning systems in sparse forest plots [8,29,30]. Studies have shown that stem detection rates decrease in more complex forest plots with a higher stem density and a lot of understory vegetation [8,28–31]. Additionally, the detection rate of spruces is often significantly lower than that of pines [8,29,30].

In addition to the high success rate of tree detection, under-canopy laser scanning systems have been demonstrated to estimate tree attributes with a high accuracy. Multiple studies have found that MLS methods can estimate DBH with a root-mean-square error (RMSE) ranging from 0.6 to 3.1 cm when using either TLS or manual field measurements as reference [8,13,15–17,27–29,32]. However, the DBH estimates provided by under-canopy MLS systems tend to be less accurate for smaller trees with a DBH below 10 cm [13,15,28]. For tree height estimation, MLS methods have achieved RMSEs of 0.4–2.0 m [7,8,29,30,33]. Additionally, studies employing the same algorithmic workflow as used in this study have found that the stem curve can be estimated with an RMSE of 1.2–1.7 cm (2–15%) and the stem volume with an RMSE of 9–15% [7,8,29,30]. These results mark an improvement compared to prior research that utilized different methods, which reported RMSE values for stem curve estimates of around 15–30% and for stem volume estimates of approximately 20–50% [18,31,34].

Above-canopy ALS constitutes the fastest method for collecting laser scanning data about forests, potentially enabling the measurement of tens or even hundreds of thousands of trees in a single day [9]. With treetops being captured well and positioning errors being minimal as a result of the strong GNSS signal, ALS is particularly suitable for obtaining accurate tree height measurements. Prior studies have demonstrated that tree height estimates derived from ALS are more accurate compared to estimates based on manual field measurements, MLS, or TLS [3,18,35]. Typically, the ALS height estimates maintain high accuracy across various tree heights, species, forest complexities, and stem densities. Meanwhile, previous research has found variable accuracies when using ALS to estimate other attributes of individual trees. Several studies have found RMSEs for DBH estimates in the range of 4–8 cm [14,18,36–38]. Using high-density ALS point clouds, Hyyppä et al. [9] improved the accuracy to 2–3 cm (6–10%) by automatically detecting stem arcs, i.e., horizontal clusters of laser hits to the tree stem obtained during a brief period of time. The RMSE of stem volume acquired was 13–21% while detecting 42–71% of the trees in the studied plots. However, the overall vertical coverage of trees can be limited when using above-canopy laser scanning, which may hinder stem detection. Along with the overall lower stem detection rate compared to TLS and MLS systems, the completeness decreases even more with increasing forest complexity [18]. The tree size is also an important factor affecting the completeness rate, as ALS has been found to detect 85–100% of trees with a DBH larger than 20 cm, whereas smaller trees were detected with a much lower completeness rate [9]. Nevertheless, field reference measurements are only required from a section of trees in a plot [39] when implementing an individual-tree-based forest inventory. Thus, the accuracy of the attribute estimates from a portion of trees representative of the plot can be prioritized.

In contrast to the kinematic laser scanning approaches, TLS provides a static platform from which various individual tree attributes can be measured without distortions induced by motion. Therefore, the stem curve and DBH can be estimated at a higher precision, at an RMSE of approximately 1–2 cm [6,10,40–42]. Stem volume has been found to be estimated with an RMSE of approximately 10% in sparser plots using TLS, with the estimates being as accurate as using the best national allometric model available [6]. The combination of TLS and above-canopy laser scanning has also been studied and suggested to be an optimal method for collecting data on individual trees [7,32,43–47]. This approach can utilize the detailed point cloud data of treetops from the above-canopy laser scanning and the detailed point cloud data of tree stems from the TLS platform. The combination of ALS-derived tree height and TLS-derived stem curve has been expected to provide the most accurate technique today to produce stem volume estimates in easy and more complex forest plots [7].

The main limitations of TLS include the longer data collection duration, the required point cloud registration techniques, as well as occlusion issues that hinder the visibility of treetops and tree stems. Even though producing a single scan using TLS only takes approximately one minute today, setting up each individual scan takes a prohibitive amount of time when obtaining a large-area forest inventory, unlike kinematic laser scanning methods and, in particular, ALS [48]. Occlusion issues originating from understory vegetation, tree branches, and other tree stems have been found in various studies to limit the accuracy of estimated tree attributes while also leading to underestimation of tree height [3,10,35,42]. Specifically, Wang et al. [3] observed systematic underestimation in the height of trees taller than 15–20 m. Occlusion in TLS-based approaches can also limit the completeness of stem detection, necessitating the use of multiple scans for each test site. The completeness of stem detection using multi-scan TLS has been found to range from around 50% to 97% [10,42,49,50]. Notably, the completeness of stem detection varies with the complexity and stem density of the forest plot, and smaller trees with DBHs less than 15 cm are often omitted in stem detection [10]. Various studies have also shown that MLS systems can detect tree stems at a higher completeness than multi-scan TLS [13,16,17], since MLS systems collect data from the same trees from a higher number of locations than TLS.

2.2. Test Area

We utilized six 32 m × 32 m test sites in our comparison, located in Evo in southern Finland (61.19°N, 25.11°E). The test sites were part of a managed natural boreal forest and consisted mainly of Scots pine (*Pinus sylvestris* L.), Norway spruce (*Picea abies* (L.) H.Karst.), Silverbirch (*Betula pendula* Roth), downy birch (*Betula pubescens* Ehrh.), and aspen (*Populus tremula*, L.). A few other deciduous trees were also present. The test sites were a part of SCAN FOREST research infrastructure [51]. The test sites were classified into two different complexity categories referred to as *easy* and *difficult* based on stem density, tree species, and stem occlusion caused by vegetation. The same complexity categories have been used in previous work [10,18,50]. However, we included one plot classified as *medium* in Liang et al. [10] into the category *difficult*, due to the *medium* plot sharing many similarities with the *difficult* plots.

Plots in the *easy* category had a tree density of approximately 500 trees/ha, while the corresponding density in the *difficult* category was 1000–2000 trees/ha. Figure 1 presents point clouds and photographs of *easy* and *difficult* plots, whereas Table 1 presents the tree species distribution in each category along with the mean value for DBH, tree height, and stem volume. Out of the tree species present in the studied boreal forest sites, the stem curve is generally the easiest to estimate for pine trees, as their stem tends to be straight with low occlusion at the lowest part of the stem. Spruces also have a straight stem, but the lower part of their stem is often heavily obstructed by branches and needles, especially for small spruces. Deciduous trees often have curved and less uniform stems, and they can have broad leaves obstructing the stem.

Table 1. Mean plot statistics for the studied complexity categories *easy* and *difficult*. Small trees were defined as having a DBH of 5–10 cm. Trees smaller than that were considered as undergrowth vegetation. The calculated mean attribute values included all detected trees in the plots, including the small trees.

	Easy	***Difficult***
Number of Plots	3	3
	Mean tree count/plot	
Pine	46	2
Spruce	2	83
Deciduous	2	71
Small Trees (DBH < 10 cm)	8	47
Total	50	156
	Mean attribute values	
DBH (cm)	22.03	18.95
Height (m)	18.94	20.93
Stem volume (m^3)	0.42	0.42

2.3. Acquisition of the Point Clouds

2.3.1. Acquisition of the Under-Canopy Point Clouds

The under-canopy laser scanning systems compared in this paper were a Zeb Horizon handheld scanner (GeoSLAM, Nottingham, UK), a system by Hovermap (2020 version, Emesent, Milton, Australia), a system by Deep Forestry (Deep Forestry, Uppsala, Sweden), and two in-house-developed handheld systems as presented in Table 2a. The Hovermap and Deep Forestry systems were mounted on a UAV. Thus, they are abbreviated as H-UAV and DF-UAV, respectively, in the remainder of this manuscript. The H-UAV system was equipped with a Velodyne VLP-16 laser scanner (Velodyne Lidar, San Jose, CA, USA, datasheet: Velodyne Lidar [52]), while the DF-UAV system utilized an Ouster OS0-32 Rev. 5 laser scanner (Ouster, San Francisco, CA, USA, datasheet: Ouster [53]). The data sets were collected under our supervision in September 2021 for the H-UAV system and in September 2022 for the DF-UAV system. This collection occurred during leaf-on forest conditions. The data were processed into point clouds with the proprietary software provided by each company. Both UAVs were capable of autonomous flight. However, due to technical issues, the DF-UAV was flown manually. Neither UAV could fly in the *difficult* plots characterized by a high stem density (see Table 1), due to DF-UAV and H-UAV requiring 2 m- and 3 m-wide gaps, respectively, for autonomous flight. Manual flight was also deemed too risky. Therefore, in the *difficult* plots, the DF-UAV drone was carried by the operator inside the plot, and the H-UAV was flown along a nearby road outside of the test plot. While the extra vibrations caused by the operator's hand should not significantly affect the results for DF-UAV, the results for H-UAV were poor as the data was not collected within the test site. Thus, we decided to discard the results of the H-UAV system for the category *difficult* plots from the comparison.

The handheld Zeb Horizon system was equipped with a similar rotating Velodyne VLP-16 laser scanner as the H-UAV system. The captured raw data were processed with GeoSLAM Hub 6.1 software with forest mode enabled for SLAM-processing and exported to point cloud in LAZ format. We collected the Zeb Horizon data in April 2020, which occurred during leaf-off foliage conditions.

The two remaining handheld scanner systems were developed in-house, and both had an Ouster OS0-128 laser scanner and a Lord Microstrain 3DM-GQ7 (MicroStrain, Williston, VT, USA) GNSS/inertial navigation system unit. The only hardware difference was that one used a Rev. C [54] and the other a Rev. 7 version of the laser scanner (datasheets: Ouster [54], Ouster [55]), respectively. The Rev. 7 is the newer version, with an improved scanning range and accuracy at the expense of some precision. Furthermore, it is capable of recording more points and dual returns, but the second returns were excluded from

the resulting point clouds. The systems are named FGI-HH-C and FGI-HH-7, respectively. The data sets were collected in July 2023 for the FGI-HH-C and in June 2023 for the FGI-HH-7 system. The foliage conditions during these times were leaf-on. The point clouds were assembled from the raw measurements by an in-house-developed positioning and mapping software processed with real-time limitations, based on SLAM and normal distribution transformation, and relying only on the laser scanner and the inertial measurement unit measurements without the aid of GNSS [26]. Figure 2b illustrates a typical measurement trajectory within a single test site for the studied MLS systems. Key properties for the studied MLS systems are provided in Table 2b.

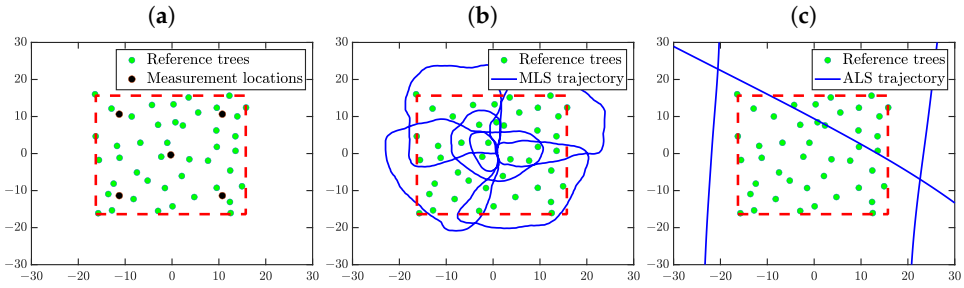

Figure 2. Illustration of the data collection for each type of laser scanning system considered in this work, including TLS (used for reference measurements), under-canopy MLS, and above-canopy ALS. The plot limits are presented as red dashed lines, while the locations of trees are shown with green circles. For TLS, the measurement locations are shown with black circles, while the trajectory for the kinematic systems is shown with a blue line. Units are meters, and the coordinates are centered to the mean of tree locations. (**a**) TLS setup. (**b**) Typical MLS trajectory. (**c**) ALS trajectory.

Table 2. Overview of the studied laser scanning systems and their scanner properties. Here, the TLS system provides the reference for DBH and stem curve, while the HeliALS system provides the reference for tree height. For the comparison of tree attribute estimation accuracy, we use the systems ZB-HH, H-UAV, DF-UAV, FGI-HH-7, FGI-HH-C, and HeliALS-TW.

(**a**) Overview of the laser scanning systems.

Name	Abbreviation	Laser Scanner	Platform	Collected
TLS	TLS	Leica RTC 360	Tripod	April 2020 *
Zeb Horizon	ZB-HH	Velodyne VLP-16	Handheld	April 2020 *
Hovermap	H-UAV	Velodyne VLP-16	Drone	Sept. 2021
Deep Forestry	DF-UAV	Ouster OS0-32 Rev. 5	Drone	Sept. 2022
FGI handheld 7	FGI-HH-7	Ouster OS0-128 Rev. 7	Handheld	June 2023
FGI handheld C	FGI-HH-7	Ouster OS0-128 Rev. C	Handheld	July 2023
HeliALS-TW	HeliALS	Riegl VUX-1HA	Helicopter	June 2021

(**b**) Properties of the studied laser scanners.

Scanner	Pulse Repetition Rate [kHz]	Range [m]	Beam Width at Exit (at 10 m) [mm]	Divergence [mrad]
Leica RTC 360	2000	130	6 (11)	0.5
Velodyne VLP-16	18.08	100	12.7 (42.7)	3.0
Ouster OS0 Rev. 5	20.48	50	5 (66)	6.1
Ouster OS0 Rev. 7	20.48	100	5 (66)	6.1
Ouster OS0 Rev. C	20.48	50	5 (66)	6.1
Riegl VUX-1HA	1017	135	4.5 (9.5)	0.5

* Leaf-off conditions.

2.3.2. Acquisition of the ALS Point Clouds

The ALS point clouds were collected in June 2021 with an in-house developed, helicopter-mounted laser scanner system called HeliALS-TW, abbreviated as HeliALS in this work. The foliage conditions at the time of collection were leaf-on. The system uti-

lized a Riegl VUX-1HA (Riegl GmbH, Horn, Austria, datasheet: RIEGL [56]) laser scanner in conjunction with a positioning system consisting of a NovAtel (LITEF) ISA-100C inertial measurement unit, a NovAtel PwrPak7 GNSS receiver, and a NovAtel (Vexxis) GNSS-850 antenna. Selected important properties of the VUX-1HA laser scanner are presented in Table 2b. The measurement flight was flown in a grid pattern with a line separation of approximately 50 m at roughly 80 m above the ground with a planned velocity of 9.5 m/s. The scanner was angled 15° forwards in the flying direction with respect to the vertical orientation. A typical flight pattern over a plot is demonstrated in Figure 2c. A virtual Trimnet VRS service (RINEX 3.04) GNSS base station, located approximately in the middle of the measured area, was used to enhance the trajectory calculations performed with the Waypoint Inertial Explorer software (version 8.9, NovAtel Inc., Calgary, AB, Canada).

2.3.3. Acquisition of the Reference Data

The main reference data were collected in April 2020 with a five-point multi-scan TLS measurement using a Leica RTC 360 laser scanner (Leica Geosystems, Heerbrugg, Switzerland, datasheet: Leica Geosystems [57]). The data collection occurred during leaf-off forest conditions. The scanning resolution was set to 6.3 mm at a 10 m distance. The setup is schematically illustrated in Figure 2a. The scans were registered and merged with Leica Cyclone 9.1 software by utilizing approximately six artificial spheres with a diameter of 198 mm attached to trees around the plot.

The TLS point clouds were used to obtain the ground truth for stem curve and DBH in this study. Furthermore, the TLS-derived stem curves were further used to compute the reference volume together with ALS-derived height according to Equation (3) presented in Section 2.4. We used the ALS height measurements as ground truth due to the superior accuracy compared to under-canopy laser scanning or even manual field measurements, as observed in previous studies [3,33,58,59]. TLS measurements have also been established as a source of accurate stem attributes, rivaling manual field measurements [6,10,40–42]. The same automatic process was used for all laser scanning systems to process the point clouds and to derive all the tree attributes used in this study, including the reference. The process is described in Section 2.4. The corresponding trees between the datasets were determined automatically based on the tree locations by using a registration algorithm proposed by Hyyppä et al. [60].

However, the stem curve extraction method used in this study has not been tested on TLS data previously. Therefore, we validated the accuracy of our method for TLS data by evaluating its performance on data sets from the international TLS benchmark described in Liang et al. [10]. For this validation, we used our method to process the TLS data from Liang et al. [10], obtaining stem curves for the detected trees. As presented in the results in Appendix A, we compared the completeness of stem detection and the accuracy of stem curve estimates to those based on the method by Liang et al. [31], which was among the most accurate methods included in the benchmark study. The stem curve reference used in the benchmark study had been obtained manually from TLS point clouds and included small trees down to a DBH of 5 cm. However, in our study, the estimated stem diameter was limited to a minimum of 8 cm for the MLS data in order to avoid false detection of trees, as discussed further in Section 2.4. For a fair comparison, the same minimum diameter threshold was used when processing the TLS data for the validation. Therefore, in order to obtain a completeness value including only trees relevant to the present study, we removed all reference trees from the benchmark dataset that did not have at least two diameter measurements larger than 8 cm along the stem before using Equation (5) to evaluate the completeness rate.

2.4. Stem Curve Extraction

In this section, we briefly describe the algorithm used to automatically detect the individual trees and to calculate their tree attributes, including DBH, height, volume, location, and stem curve. The algorithm was developed in Hyyppä et al. [7] for 2D mobile

laser scanning systems, adjusted for 3D systems in Hyyppä et al. [30], and for ALS in Hyyppä et al. [9]. As this study includes 3D mobile systems and an ALS, the reader is directed to the latter two papers for more detailed descriptions of the algorithm. Due to a significantly lower point density, especially at stem level, and higher noise level, the HeliALS data had to be processed with slightly adjusted parameter values that accept clusters of stem points as stem arcs even in the presence of a lower number of points and with a higher level of noise. The parameters we used were mostly based on the aforementioned papers, and we present the parameters that were changed and/or have different values for MLS and HeliALS in the following short description of the algorithm. The parameter values for HeliALS are presented in parentheses.

The point clouds were pre-processed by segmenting the ground, individual trees, and removing clear outliers. The ground was segmented with a simple voxel-based algorithm, in which the point cloud was divided into 2-by-2 m voxels, each with a height of 1.5 m. For each vertical stack of voxels, the ground was calculated as the average of the z-coordinates of the points in the lowest voxel containing at least 0.5% of the total points in the stack. The final digital terrain model (DTM) was obtained with Gaussian smoothing. The point cloud was then segmented into segments containing preferably only one tree using a watershed algorithm-based method [61]. The segmenting does not affect the outcome of the algorithm, but it significantly reduces the computation time of the subsequent steps. In order to avoid issues with over-segmentation, trees from neighboring segments that were closer to each other than the their average diameter at a height of 5 m were combined into a single tree.

The main part of the algorithm consists of first detecting clusters of points that potentially correspond to hits to the tree stems, called arcs, and subsequently clustering the high-quality arcs into stems. Before the arc detection, the point cloud was divided into bins based on the height above the ground and the time stamp. We used bin widths of 0.4 (1.0) m and 3 (5) s for MLS(ALS) systems. The arcs from each bin were detected by using a density-based clustering algorithm (DBSCAN, [62]). We demanded that a core point must have at least 9 (3) points within 75 mm. A circle was fitted to the arcs utilizing a random sample consensus (RANSAC, [63])-based method. For the arc to be accepted, we required it to have at least 35 (10) points and 80 (75)% of its points within 30 (35) mm of the fitted circle. We removed the noise points from the edges by dividing the arcs into sub-arcs if the center angle between neighboring points exceeded 10°(30°). The divided arcs were then either accepted or rejected based on set quality criteria. We required the arcs to contain more than 35 (10) points and have a diameter between 8 cm and 80 cm, a central angle of at least 60°, and a standard deviation of radial residuals less than 12.5 mm.

After all the bins were processed, we clustered the arc center points into trees by again utilizing DBSCAN, where we required the core points to have at least 5(2) neighboring arc centers within 25 cm. In addition, the arc centers were required to span at least 1 m in vertical distance to form a tree. Note that a segment can contain multiple trees. The tree growth direction was determined with principal component analysis (PCA), and the estimated arc radii were adjusted by projecting the arcs to a plane perpendicular to the growth direction. Here, we deviated from Hyyppä et al. [29] and applied our method to reduce the bias caused by the beam width of the laser pulses. The arc diameters were adjusted based on the calibrated parameters and the measurement distance. The bias calibration method is discussed in more detail in Section 2.5. For the TLS reference, this step was skipped, as the bias from the beam width in TLS is negligible due to the small divergence and short measurement distance, see Table 2b. In addition, the calibration requires a reference that is more accurate than the method, and creating a reference more accurate than TLS is extremely time-consuming and difficult. To calculate the stem curve, the arcs corresponding to a single tree were divided into 40 cm intervals along the z direction from $z = 0.5$ m up to the z coordinate of the highest extracted arc, and clearly outlying diameter estimates were removed with the method presented in Hyyppä et al. [7].

We obtained the stem curve by fitting a cubic smoothing spline to the mean diameter estimate of each interval.

The tree height was estimated by including all points within 75 cm of the center of the tree and dividing them into 50 cm height intervals. From this point onward, the height was calculated differently for large, dominant trees and small, suppressed trees, due to the possibility of large trees having branches above the small trees. A large tree was defined as a tree with a stem diameter larger than 20 cm at some height, and the top was determined to be in the highest height interval containing at least 5 points. For small trees, the treetop was determined as one interval below the interval that was the lowest interval containing less than 10 points but still above the highest extracted stem arc. For both cases, the final tree height was estimated as the average of the five highest points in the interval containing the treetop.

The stem volume was calculated by first performing a least square fit of the stem radii as a function of height data, z, to a parabola

$$R_1(z) = a_1(h-z)^2 + a_2(h-z) \tag{1}$$

and to a square root function

$$R_2(z) = b_1\sqrt{h-z}, \tag{2}$$

where h denotes the height of the tree, and a_1, a_2, and b_1 are parameters obtained from the fit. The stem volume, V, is then calculated by integrating both Equations (1) and (2) and taking the average as

$$V = \frac{\pi}{2}\left(\int_0^h R_1(z)^2 \mathrm{d}z + \int_0^h R_2(z)^2 \mathrm{d}z\right). \tag{3}$$

2.5. Bias Compensation

Laser scanners overestimate the radius of cylindrical objects due to the non-zero beam width of the laser pulse [64]. For sufficiently small divergence angles, the beam width d depends approximately linearly on the distance x between the object and the scanner as $d = d_{\text{exit}} + x\theta$, where d_{exit} is the beam width at exit. For high-quality scanners that are operated near the measured trees, as was the case in Hyyppä et al. [7,29], this phenomenon is thus negligible. However, for typical scanners used in mobile laser scanning systems, the beam can be several centimeters wide at the typical measurement distance of 5–10 m. The lower quality beams are used in order to fit more beams into the system and thus obtain a 3D view of the surroundings, which makes the SLAM algorithm used for positioning much more effective [65]. Even a high-quality scanner can have a large footprint at long measurement distances, as is the case with the HeliALS system. Figure 3a illustrates the effect of the beam width on the detection of cylindrical objects, in this case trees.

To date, the attempts made at compensating the bias have been limited in the literature. Ringdahl et al. [66] proposed a correction angle depending on the beam width, that shifts points within the arc towards the center of the arc. Forsman et al. [64] simulated laser pulses hitting cylindrical objects and found a near-quadratic relation between the overestimation of the cylinder radius and the beam width. However, as demonstrated by Figure 3b, we find that the noise in the diameter measurements in a natural forest is significantly higher than the deviation between a linear and a quadratic least squares fit, which was at most 2 mm and on average 1.2 mm for the illustrated Deep Forestry data. As presented in Table 2b, the Ouster OS0 scanner used by Deep Forestry has the highest divergence in this comparison, and thus the strongest dependence between the beam width and the scanning distance. Therefore, we chose to use a linear model in order to reduce the number of fitting parameters and thereby avoid over-fitting due to outliers. This is especially important for the ALS system, for which the beam divergence is small, but the footprint is relatively large due to the long measurement distance. The linear model is also supported by a recent Zeb Horizon noise analysis by Kuželka and Surový [67].

The calibration of parameters for the bias compensation was performed on a single plot in the *easy* category that was excluded from the rest of the comparison. After extracting the stem curves of detected trees as described in Section 2.4, we compared the radius estimates of each individual arc to the reference stem curve and calculated the difference as well as the distance to the scanner trajectory, as shown in Figure 3b. The corresponding trajectory point was determined by calculating the average time stamp of the arc points and matching it with the nearest trajectory time stamp. The location of the arc was defined as the center of the circle fitted to it. Ideally, the correction would be conducted at the individual point level, but due to the temporal segmentation to a few second segments, the distance differences within the arc were small. Finally, a linear model of the form

$$\Delta D(x) = ax + c \tag{4}$$

was fitted to the collected data using a linear least squares model, with $\Delta D = D_{\text{arc}} - D_{\text{ref}}$ denoting the difference between the arc and the reference stem curve diameters and a and c representing the parameters to be calibrated according to the fit. After the calibration of the parameters a and c, the diameter estimates for the arcs in the other plots were bias-corrected by subtracting Equation (4) from them. In addition to calibrating out the bias caused by the beam width, this method also partially negates the bias caused by tree growth over the three years that the measurements spanned, as the average growth is captured by the constant parameter c.

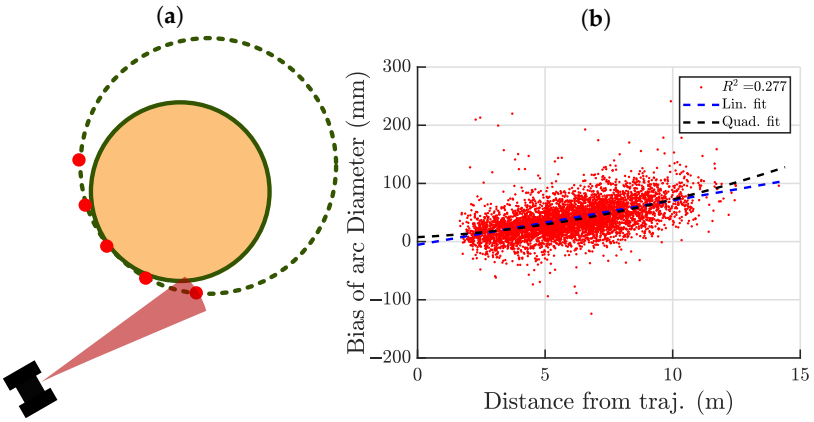

Figure 3. Illustration of the bias compensation. (**a**) Illustration of the beam width affecting the measured circle radius. The red dots illustrate the measured points, and the dashed circle is the circle fitted to them. The beam divergence is greatly exaggerated for this illustration. (**b**) Example fit to the diameter bias–distance to the trajectory data for the DF-UAV. The red dots represent the diameter of a circle fitted to each individual arc. A linear and quadratic least square fit is illustrated with a black and blue dashed line, respectively. The calibration was performed using a single *easy* plot with TLS as a reference.

2.6. Evaluation Metrics

For an individual-tree-level forest inventory, accurate tree attributes are crucial, as are the tree detection rate and correctness. In this section, we describe the metrics used for evaluating them. We evaluated the stem detection rate of the laser scanning systems using completeness and correctness, defined as

$$\text{Completeness} = \frac{\text{Number of detected reference trees}}{\text{Number of reference trees}}, \tag{5}$$

$$\text{Correctness} = \frac{\text{Number of detected reference trees}}{\text{Number of detected trees}}. \tag{6}$$

For the tree attributes, we evaluated the DBH, volume, and height, as well as the stem curve, which is an extension of the DBH and provides the diameter of the stem at

different heights. The quality of the tree attributes was evaluated by utilizing bias, root-mean-square error (RMSE), median absolute error (MAE), as well as the standard deviation of the measurement error (Error sd.). They are given by

$$\text{bias} = \sum_{i=1}^{N} \frac{x_i - x_{i,\text{ref}}}{N}, \tag{7}$$

$$\text{RMSE} = \sqrt{\sum_{i=1}^{N} \frac{(x_i - x_{i,\text{ref}})^2}{N}}, \tag{8}$$

$$\text{MAE} = \text{median}(\{|x_i - x_{i,\text{ref}}|\}_{i=1}^{N}), \tag{9}$$

$$\text{Error sd.} = \sqrt{\text{RMSE}^2 - \text{bias}^2}, \tag{10}$$

where N is the number of matching tree attributes, and x_i and $x_{i,\text{ref}}$ denote the tree attribute estimate and the corresponding reference value, respectively. For DBH, volume, and height, N is the number of matching trees between the evaluated and the reference data sets, and for stem curves, it is the sum of matching heights (from the ground), at which the stem curve could be estimated for both the reference and the evaluated system. The relative error can be calculated from the absolute errors (Equations (7)–(10)) by dividing them with the mean of the reference value.

3. Results

3.1. Stem Detection

Figure 4 presents the results for the completeness and correctness of stem detection with respect to the TLS reference. Completeness (Equation (5)) was approximately 90–100% for all MLS devices in the *easy* plots and around 80% in the *difficult* plots, with the exception of FGI-HH-C which had a completeness of 66% in the *difficult* plots. HeliALS had a significantly lower completeness of 54% and 17% in the *easy* and *difficult* plots, respectively. Meanwhile, the correctness (Equation (6)) of stem detection was close to 100% for all devices in the *easy* plots and approximately 80–90% for the MLS systems in the *difficult* plots. HeliALS had the highest correctness rate in the *difficult* plots at 98%, which is most likely due to the very low completeness rate caused by its inability to detect small trees that are abundant in the *difficult* plots.

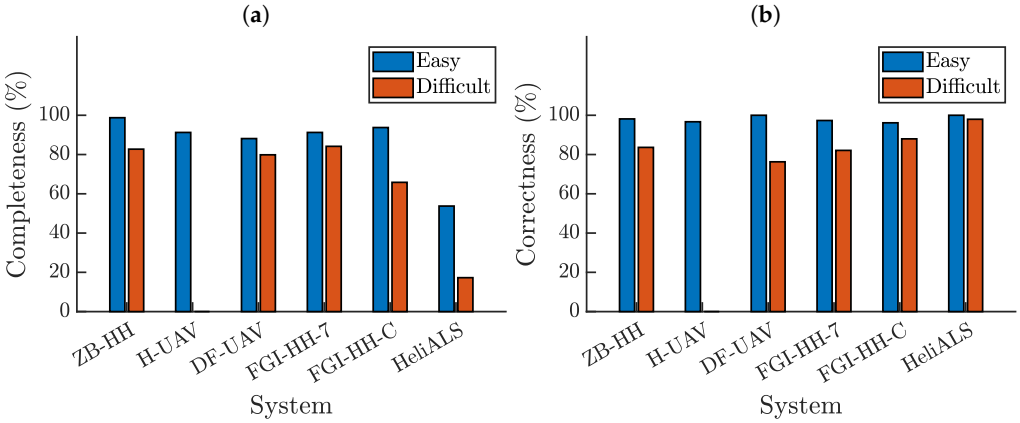

Figure 4. Stem detection statistics. The completeness and correctness (Equations (5) and (6)) were evaluated with respect to the trees found from the TLS data. The estimated completeness of the TLS for differently sized trees is presented in Figure A1c. The correctness of the trees found automatically from TLS was manually confirmed. (**a**) Completeness of the stem detection. (**b**) Correctness of the stem detection.

3.2. Accuracy of the Tree Attribute Estimation

3.2.1. Accuracy without the Bias Compensation

This section presents the accuracy of the tree attribute estimation without the bias compensation outlined in Section 2.5. Figures 5 and 6 present the results for the categories *easy* and *difficult*, respectively. In the *easy* category, the RMSEs of the DBH and stem curve estimates were around 5–10%, and approximately 20% for the stem volume for the VLP-16-based ZB-HH and H-UAV systems. For the Ouster OS0-based systems, the RMSEs of the DBH and stem curve estimates were around 15–25%. The RMSE of the stem volume was around 30%, with the exception of FGI-HH-7, which had an RMSE of about 50%. Without the bias compensation, the differences between the VLP-16 and Ouster OS0 scanners were noticeable. With Ouster OS0-family scanners having more than double the beam divergence (1.5–3 mrad compared to 6.1 mrad) of the VLP-16, these scanners heavily overestimated stem diameter. Furthermore, the older OS0 versions 5 and C systematically underestimated the tree heights. The poor performance of FGI-HH-7 in the stem volume was due to it seeing the treetops better than the older OS0 models, and thus overestimation of the stem diameter was not compensated by underestimation of the tree height.

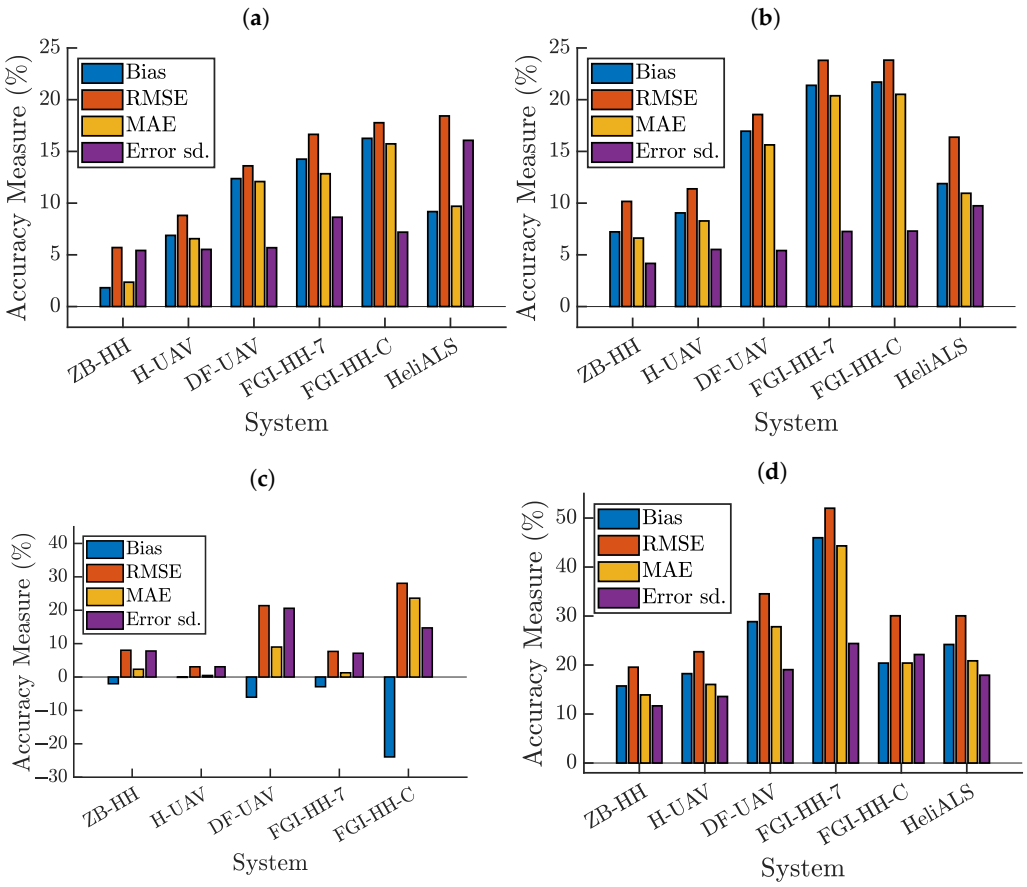

Figure 5. Accuracy of tree attribute estimation in category *easy* plots without the bias compensation. (**a**–**d**) depict the relative errors of DBH, stem curve, height, and stem volume, respectively. For each device, the bias, RMSE, MAE, and the standard deviation of the error (Equations (7)–(10)) are presented from left to right as colored bars. (**a**) DBH in *easy* plots. (**b**) Stem curve in *easy* plots. (**c**) Height in *easy* plots. (**d**) Stem volume in *easy* plots.

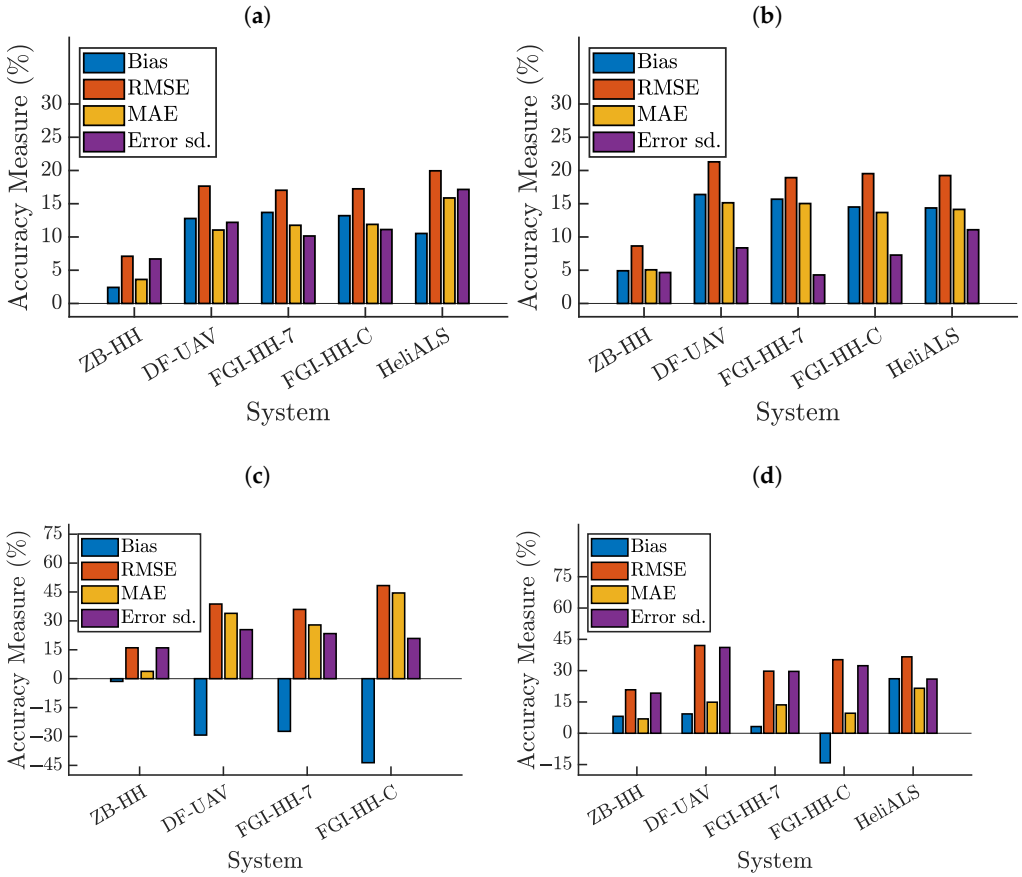

Figure 6. Accuracy of tree attribute estimation in category *difficult* plots without the bias compensation. (**a**–**d**) depict the relative errors of DBH, stem curve, height, and stem volume, respectively. For each device, the bias, RMSE, MAE, and the standard deviation of the error (Equations (7)–(10)) are presented from left to right as colored bars. (**a**) DBH in *difficult* plots. (**b**) Stem curve in *difficult* plots. (**c**) Height in *difficult* plots. (**d**) Stem volume in *difficult* plots.

3.2.2. Accuracy with the Bias Compensation

The accuracy of the acquired stem attributes when bias compensation was used are presented in Figures 7 and 8 for *easy* and *difficult* plots, respectively. In the *easy* plots, the RMSEs (Equation (8)) of the stem curve and DBH were less than 10% for all MLS devices and approximately 11% for HeliALS. ZB-HH (Zeb Horizon) was the most accurate in both categories, with RMSE values of 6.6% and 4.5% for stem curve and DBH, respectively. The errors were somewhat larger in the *difficult* plots. ZB-HH was still the most accurate system with a stem curve and DBH RMSE of 7%, whereas DF-UAV and FGI-HH-7 had RMSEs of approximately 10%, FGI-HH-C of roughly 15%, and HeliALS 20%. The absolute errors for all acquired attributes are presented in Appendix B.

The accuracy of height measurements showed more deviation between the MLS systems. Note that as HeliALS was used as the reference in this category, its error could not be evaluated. The VLP-16-based ZB-HH and H-UAV provided the most accurate height measurements, at 8.0%, and 3.5% RMSE, respectively, in the *easy* plots, and ZB-HH had an RMSE of 18% in the *difficult* plots. As discussed in Section 2.3, these plots were not measured with H-UAV. The FGI-HH-7, equipped with newer model Ouster OS0 sensors, provided relatively accurate height measurements in the *easy* plots with an RMSE of 12%. However, in the *difficult* plots, it significantly underestimated the heights, leading to a negative bias (Equation (7)) of around 30% and RMSE of 40%. The underestimation was even greater with the systems equipped with older Ouster OS0 models, where the underestimation was more than 10% for DF-UAV and 25% for FGI-HH-C, even in the *easy* plots. This is reflected

in the volume estimates where FGI-HH-C, DF-UAV, and FGI-HH-7 had an RMSE of 32%, 22%, and 17% in the *easy* plots, respectively. The corresponding RMSE values were 56%, 47%, and 44% in the *difficult* plots. The RMSE was significantly lower for the MLS systems equipped with the VLP-16 scanner, which had RMSEs of approximately 10% and 20% in the volume estimates for *easy* and *difficult* plots, respectively.

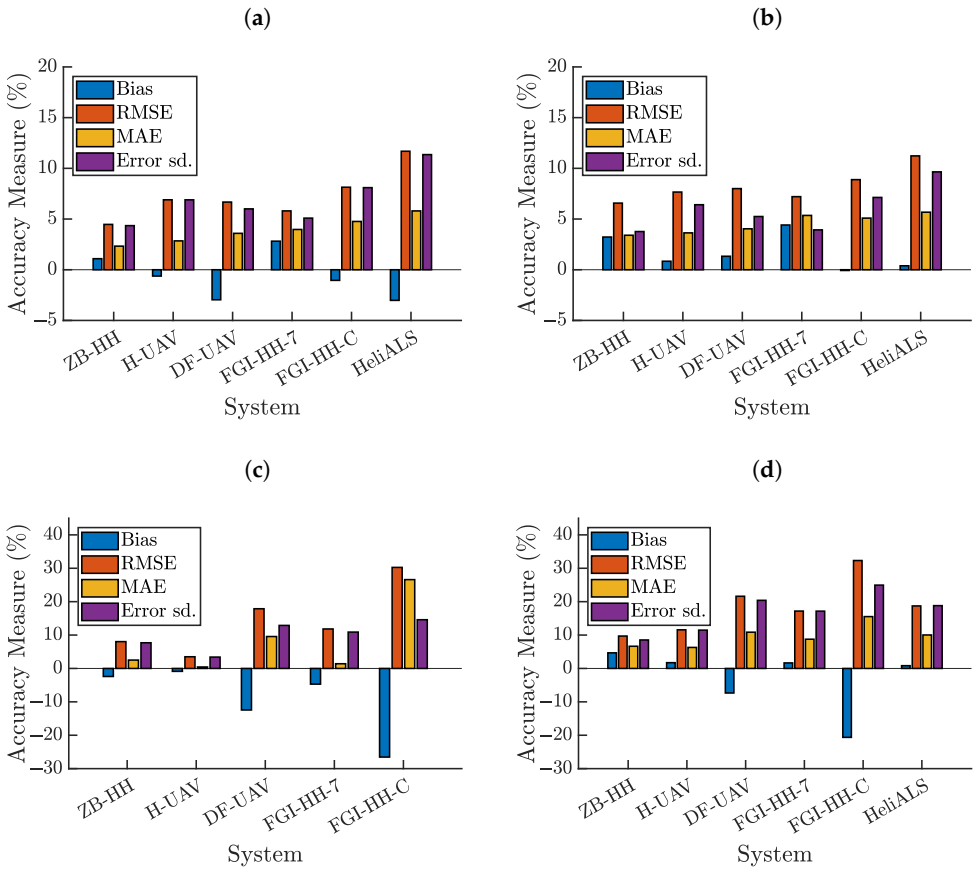

Figure 7. Accuracy of tree attribute acquisition with bias compensation in category *easy* plots. (**a**–**d**) depict the relative errors of DBH, stem curve, height, and stem volume, respectively. For each device, the bias, RMSE, MAE, and the standard deviation of the error (Equations (7)–(10)) are presented from left to right as colored bars. (**a**) DBH in *easy* plots. (**b**) Stem curve in *easy* plots. (**c**) Height in *easy* plots. (**d**) Stem volume in *easy* plots.

Table 3 presents the improvement induced by the distance-dependent bias compensation discussed in Section 2.5. The constant and slope are the parameters c and a of Equation (4), which were obtained with a least square fit to the diameter bias–scanner distance data illustrated in Figure 3. For the scanners equipped with the VLP-16 scanner, the slopes were 2.68 mm/m and 1.5 mm/m and the constants were −6.07 mm and 0.72 mm for ZB-HH and H-UAV, respectively. The VLP-16 had a vertical divergence of 1.5 mrad and a horizontal divergence of 3.0 mrad. The slopes were still noticeably different despite both scanners being mounted to similar rotating platforms, giving a full 360-degree field-of-view and even distribution of the oval-shaped beam orientations. The constants were also noticeably different from each other. The systems equipped with different versions of the Ouster OS0 laser scanner had slopes ranging from 7.00 mm/m to 8.54 mm/m and constants ranging from −3.86 mm to 4.76 mm. Compared to the VLP-16-based systems, the slopes were steeper, as expected from the divergence of 6.1 mrad. The slopes and constants were also closer to each other than to the VLP-16 scanners. HeliALS had a slope of −0.68 mm/m, which is small, as expected based on a divergence of 0.5 mrad. However, the negative sign was unexpected. The constant of the HeliALS bias was 48.14 mm, which corresponds to the beam width at roughly 87 m, which is close to the average measurement distance.

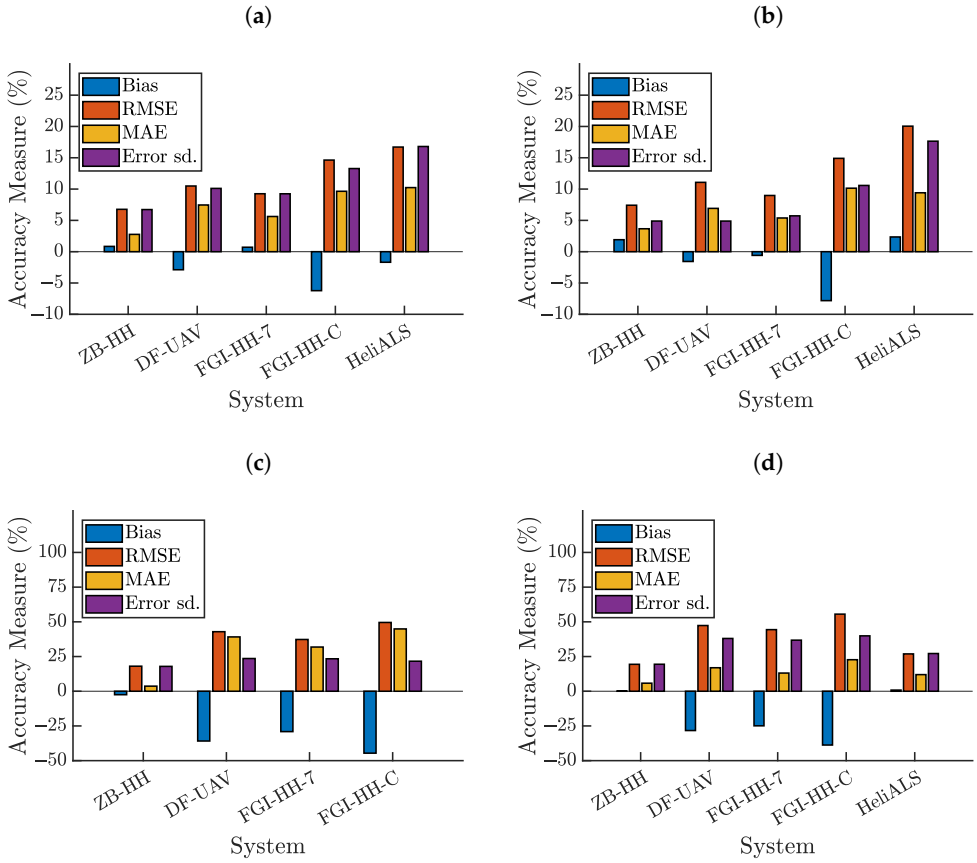

Figure 8. Accuracy of tree attribute acquisition with the bias compensation in category *difficult* plots. (**a**–**d**) depict the relative errors of DBH, stem curve, height, and stem volume, respectively. For each device, the bias, RMSE, MAE, and the standard deviation of the error (Equations (7)–(10)) are presented from left to right as colored bars. (**a**) DBH in *difficult* plots. (**b**) Stem curve in *difficult* plots. (**c**) Height in *difficult* plots. (**d**) Stem volume in *difficult* plots.

Furthermore, Table 3 presents the amount of bias removed using the bias compensation approach. Note that the bias calibration was performed on a category *easy* plot that is not a part of the results for the accuracy comparison. In category *easy* plots, 56% of the bias was removed for ZB-HH, 79% for FGI-HH-7, and 90–99% for the others. In the *difficult* plots, only 46% of the bias was removed from the FGI-HH-C results and 61% from the ZB-HH results, while 84–96% of the bias was removed from the other systems. Especially from *easy* plots, it is easy to conclude that laser scanners with large beam divergence, such as Ouster, provide large bias and, therefore, also large RMSE values. For these systems, the RMSE values were, for DBH, at the level of 15% and, for stem volume, were more than 30%. Hence, they do not meet accuracy requirements, since stem diameter and volume can be estimated with 15 and 30% accuracy, respectively, using traditional individual tree approach [58] with relatively sparse ALS data [68]. Therefore, the implementation of bias compensation is crucial for improving the accuracy of laser scanning systems, particularly when using scanners with large beam divergence.

Overall, the presented bias compensation method can eliminate most of the bias, and the calibration performed on a category *easy* plot with mostly coniferous trees can be translated well to *difficult* plots with a large number of deciduous trees. While the stem diameter bias is strongly correlated with the measurement distance, the random noise in the estimated arc diameters was quite high. Thus, more research is needed to determine the potential source of random error as well as additional bias sources and to develop methods to mitigate them. One potential source of error is the non-circular shape of the stem cross-section. This can be especially problematic for scanners that do not have a

full 360-degree view of the stems, such as TLS and ALS, and even MLS might not have stem measurements from all directions in *difficult* plots due to obstructions. Furthermore, the bias model used in this study is incomplete and did not take into account that the wide beam not only widens the stems, but also distorts them, even if the the stem itself is perfectly circular.

Table 3. Bias compensation results. Constant and slope are the parameters of the linear least square fit to the (measurement distance, diameter estimation error) data (see Figure 3).

System	Fit Parameters		Bias Removed (%)	
	Constant (mm)	Slope (mm/m)	*Easy* Plots	*Difficult* Plots
ZB-HH	−6.07	2.68	55.52	61.38
H-UAV	0.72	1.50	90.76	-
DF-UAV	−3.86	7.56	92.25	90.21
FGI-HH-7	−4.76	7.00	79.04	96.29
FGI-HH-C	−3.52	8.54	99.66	45.98
HeliALS	48.14	−0.68	96.67	83.96

3.3. Limitations and Further Developments

While the results for the tree heights were unsurprisingly worse in *difficult* plots compared to *easy* ones, it is notable that the RMSE of height measurements increased significantly more than for the stem curve in comparison to the category *easy* plots. This is probably not caused by the laser scanning systems themselves but rather by limitations in our algorithms.

Determining the tree heights is challenging in dense forest, especially for smaller trees suppressed by nearby large trees. In addition, the high tree density can obstruct the view to the tops of the large trees. To demonstrate this, we plotted the tree height error for individual trees as a function of tree height in Figure 9. We chose ZB-HH for this demonstration, as it did not systematically underestimate the tree heights. As the figure demonstrates, the height estimation accuracy does not depend on the tree height in category *easy* plots. However, in *difficult* plots, the outliers were generally overestimations for trees less than 20 m tall and underestimations for taller trees. This supports the conclusion that the tops of large trees are obstructed by the dense canopy while the locations of the treetops are ambiguous for small trees that have overlapping canopies with nearby large trees. This issue does not only affect the MLS methods, but also the ALS reference that may have higher errors for the *difficult* plots. Deep learning-based methods could help with the latter problem. However, annotating a sufficient amount of training data is laborious, as manually distinguishing which canopy belongs to which tree based on the point cloud data may be difficult even for a human. Alternatively, better traditional algorithms, such as TreeISO [69] could be used, although they can be computationally expensive and depend on carefully selected parameters that may need to be separately adjusted for each laser scanning system.

The data were collected over a period of three years, and therefore, growth of the trees affected the results of this study. A recent study by Soininen et al. [70] found that the annual DBH growth in the study area ranged approximately from 1 to 4 mm. While the bias compensation negates the average growth due to the constant parameter c in Equation (4), some error remains due to trees growing at different rates. Assuming even distribution of growths, no other error sources than the growth, and that the average growth is negated by the bias compensation, Equation (8) gives an RMSE of approximately 0.9 mm per year, which corresponds to 5–9% of the absolute DBH errors in *easy* plots for MLS systems. While this does not change the main conclusion of this paper, it is a noticeable proportion of the error, and therefore, measurements should be completed within a short time period in future studies.

While the completeness of the TLS reference is sufficient for comparing the accuracy of the stem curves, better tree detection methods are required for evaluating the absolute

detection rate of the scanners. More discussion on the reference completeness and different interpretations of completeness are presented in Appendix A. In this study, the potential trees whose stem curve could not be evaluated reliably were discarded. However, it would be beneficial to develop methods to detect those trees as well for a more complete reference and understanding of the measured forest. Furthermore, if the trees could be segmented reliably before the arc-based stem curve algorithm, it would decrease the computational cost further and avoid any potential errors caused by poor segmentation. Currently, the algorithm used in this study can usually handle situations where part of the tree is segmented into a different segment than the other part. However, it is possible that the segmentation cuts a tree in half in a way that none of the arcs meet the quality criteria anymore, and thus, the tree would not be detected.

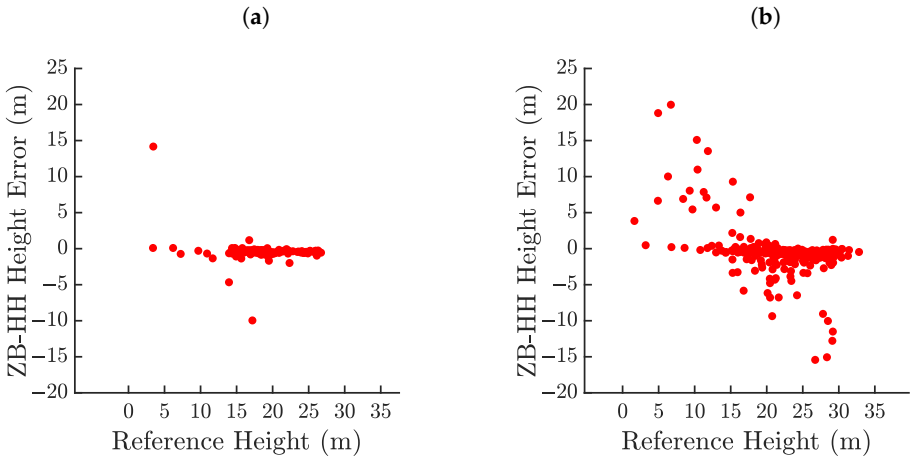

Figure 9. Demonstration of the error in the height measurements. (**a**,**b**) display the height error of ZB-HH as a function of reference tree height for category *easy* and *difficult* plots, respectively. (**a**) Height estimate error in *easy* plots for ZB-HH. (**b**) Height estimate error in *difficult* plots for ZB-HH.

4. Conclusions

We compared the stem attribute acquisition accuracy of several MLS systems and an ALS system in boreal forest plots with varying tree compositions and densities, including dense, *difficult* plots having 1000–2000 trees/ha for the first time in such a comparison. The most accurate MLS systems yielded a stem curve (and DBH) RMSE of less than 10% for all plots as well as stem volume and tree height with similar accuracy for plots categorized as *easy*. This accuracy rivals manual field measurements and is sufficient for a single-tree-level forest inventory. High-density ALS data also provided good stem curve and volume accuracy in both *easy* and *difficult* plots. However, completeness of the stem detection based on ALS data was significantly below that of any MLS system, especially in *difficult* plots, but high completeness may not necessarily be needed to collect reference data for individual-tree-based inventories, as long as a representative sample of trees is recorded. The volume estimates were equally accurate for those MLS systems equipped with a laser scanner with sufficient range to measure the treetops reliably. Our results suggest that more research is still needed to improve the tree detection rate and accuracy of the estimated tree attributes in plots determined as difficult in terms of visibility (due to vegetation density) when using MLS systems to meet the accuracy requirements for reference data collection.

Furthermore, we demonstrated that bias compensation based on the distance between the scanner and the measured tree can be used to alleviate the widening of the tree stems in the point cloud caused by the diverging laser beam. The model of the diameter bias calibrated using a single category *easy* plot translated well to other plots, including *difficult* plots where the tree composition was vastly different. Without the bias compensation, MLS systems characterized by a large beam divergence cannot measure tree attributes with the accuracy required by operative forest inventories according to our results.

Author Contributions: D.T. and J.M. acted as a joint first author, wrote the manuscript, and analyzed the data. E.H. developed the algorithms for stem detection and stem curve estimation. T.F. developed the FGI-HH systems. M.L. performed the TLS reference validation. The data were collected by T.H., H.K., A.K. and T.F. All authors participated in improving the manuscript. H.K., A.K. and J.H. acted as senior authors. All authors have read and agreed to the published version of the manuscript.

Funding: We gratefully acknowledge the Academy of Finland that funded this research through grants "Forest-Human-Machine Interplay—Building Resilience, Redefining Value Networks and Enabling Meaningful Experiences (357908)", "Feasibility of Inside-Canopy UAV Laser Scanning for Automated Tree Quality Surveying" (334002), "Capturing structural and functional diversity of trees and tree communities for supporting sustainable use of forests" (348644), "Understanding Wood Density Variation Within and Between Trees Using Multispectral Point Cloud Technologies and X-ray Microdensitometry" (331708) and the Ministry of Agriculture and Forestry that funded this research through the grant "Future forest information system at individual tree level" (VN/3482/2021). The academy-funded research infrastructure grant "Measuring Spatiotemporal Changes in Forest Ecosystem" (336382) and the European Union's Horizon Europe FEROX project grant (10107044) were also applied for the benefit of this study.

Data Availability Statement: The point cloud data collected with Zeb Horizon are available from https://www.scanforest.fi/data/ (accessed on 8 May 2024). TLS data sets collected from the same plots with the same system in 2019 and 2021 are available from the same website, along with other data sets from the same test area.

Acknowledgments: Mikko Vastaranta, University of Eastern Finland, is acknowledged as a key collaborator in the SCAN FOREST research infrastructure project.

Conflicts of Interest: The authors declare no conflicts of interest. The funders had no role in the design of the study; in the collection, analyses, or interpretation of data; in the writing of the manuscript; or in the decision to publish the results.

Appendix A. Reference Validation

In this section, we present the validation of the TLS reference data used in this study. Figure A1 presents the accuracy of our reference calculation method compared to the method by Liang et al. [31], which was among the most accurate in an international TLS benchmark study [10]. The comparison was performed on four category *easy* and three category *difficult* plots, denoted as E1–E4 and D1–D3, using TLS data, respectively. These were the same plots as used in the rest of this manuscript; E1 was used for the bias calibration, whereas the E2–E4 and D1–D3 plots were used for the rest of the comparison. The RMSE of the stem curve obtained with our method was equal or lower than that obtained with the method by Liang et al. [31] across all plots. However, the completeness of stem detection based on our method was slightly lower for the *easy* plots and for one of the *difficult* plots and was significantly lower for the two other *difficult* plots. This was caused by the large amount of small trees in those plots, as demonstrated by Figure A1c. The stem detection rate was significantly lower for small trees with a DBH less than 15 cm, whereas for larger trees, the completeness rate was around 90–100% and 80–100% for *easy* and *difficult* plots, respectively. The lower completeness in *difficult* plots was due to the occlusion caused by the high tree density. We used the same method for deriving the tree attributes for both the TLS system providing reference and the compared laser scanning systems in order to partly eliminate the effect of the stem curve algorithm from the comparison of the laser scanning systems. As the used algorithm was developed for mobile systems measuring trees from multiple angles but suffering from moderate noise and drift in their trajectory, the algorithm may not be ideal for detecting trees from TLS data.

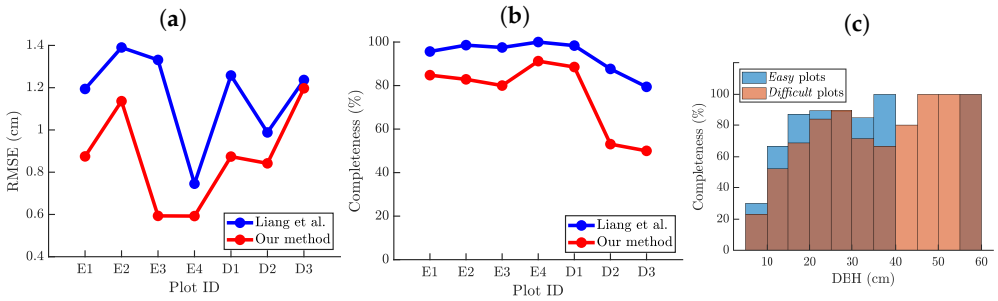

Figure A1. TLS reference accuracy evaluation. Our method refers to the method used for obtaining the stem curve reference in this paper, and Liang et al. is the method developed in [31] and evaluated in the international TLS benchmark [10], where it is referred to as the *FGI-method*, and it was one of the best-performing algorithms in the paper. The methods are compared to a reference obtained manually from the TLS point clouds. In (**a**,**b**), E1 corresponds to the calibration plot for the bias compensation, E2–E4 and D1–D3 being the *easy* and *difficult* plots, respectively, presented in Table 1. For (**c**), the completeness with respect to DBH in *easy* and *difficult* plots is depicted with colored bars, with blue illustrating *easy* plots, light red illustrating *difficult* plots, and the overlap of the two bars appearing as dark red/brown. Note that there were no trees with a DBH of 40–55 cm in the *easy* plots. Details can be found in Section 2.3.3. (**a**) RMSE of the stem curve. (**b**) Completeness of the stem detection. (**c**) Completeness with respect to the tree size.

As a result of the omission of small trees in the TLS reference produced using our method, the completeness rates of the kinematic laser scanning systems evaluated with respect to the TLS reference may overestimate the true completeness rate. However, this does not prevent us from comparing the relative performance between the different systems. Importantly, the completeness rate can be interpreted to measure two metrics. In an absolute sense, it measures the tree detection rate, which is affected by the scanner hardware, trajectory, and the applied stem detection algorithm and its parameters. In a relative sense, it measures the reliability of other accuracy metrics, such as the RMSE of the stem curve. Typically, the trees that are more difficult to detect are small and irregularly shaped, making accurate measurement of their attributes more challenging. Consequently, when comparing multiple scanners, the results regarding estimated tree attributes are only well comparable if their completeness rates are of similar magnitude. As this study mainly concentrates on comparing laser scanning systems, measuring the completeness with respect to a reference produced with TLS is thus sufficient. In addition, the mobile scanners also have difficulties detecting small trees due to the noise and motion distortions. Our reference collection method could extract most tree stems that the mobile scanners could, which is reflected in the high correctness values presented in Figure 4. Therefore, we conclude that our reference collection method is suitable for use as a reference for mobile laser scanners in this study. However, the method should be improved to provide a higher completeness rate for TLS data in the future.

Appendix B. Relative and Absolute Errors for Tree Attribute Estimation Using Bias Compensation

In this section, we present the relative and absolute accuracy of the tree attribute estimation when bias compensation was used in Tables A1 and A2 for *easy* and *difficult* plots, respectively.

Table A1. Accuracy of tree attribute estimation with bias compensation in *easy* plots.

System	Attribute	Bias	Bias (%)	RMSE	RMSE (%)
ZB-HH	DBH (cm)	0.2	1.1	1.0	4.5
	stem curve (cm)	0.6	3.2	1.3	6.6
	height (m)	−0.5	−2.4	1.5	8.0
	volume (m^3)	0.02	4.7	0.04	9.7
H-UAV	DBH (cm)	−0.1	−0.6	1.6	6.9
	stem curve (cm)	0.2	0.8	1.6	7.7
	height (m)	−0.2	−0.9	0.7	3.5
	volume (m^3)	0.008	1.7	0.05	11.6
DF-UAV	DBH (cm)	−0.7	−3.0	1.5	6.7
	stem curve (cm)	0.3	1.3	1.7	8.0
	height (m)	−2.4	−12.4	3.5	17.9
	volume (m^3)	−0.03	−7.4	0.1	21.6
FGI-HH-7	DBH (cm)	0.6	2.8	1.3	5.8
	stem curve (cm)	0.9	4.4	1.5	7.2
	height (m)	−0.9	−4.7	2.3	11.8
	volume (m^3)	0.007	1.7	0.08	17.2
FGI-HH-C	DBH (cm)	−0.2	−1.0	1.8	8.1
	stem curve (cm)	−0.02	−0.07	1.9	8.9
	height (m)	−5.1	−26.5	5.8	30.3
	volume (m^3)	−0.09	−20.6	0.1	32.3
HeliALS	DBH (cm)	−0.8	−3.0	2.9	11.7
	stem curve (cm)	0.09	0.4	2.5	11.2
	height (m)	-	-	-	-
	volume (m^3)	0.004	0.8	0.1	18.7

Table A2. Accuracy of tree attribute estimation with bias compensation in *difficult plots*.

System	Attribute	Bias	Bias (%)	RMSE	RMSE (%)
ZB-HH	DBH (cm)	0.2	0.8	1.4	6.8
	stem curve (cm)	0.4	1.9	1.4	7.4
	height (m)	−0.5	−2.5	3.9	18.0
	volume (m^3)	0.0007	0.1	0.09	19.4
DF-UAV	DBH (cm)	−0.6	−2.9	2.2	10.5
	stem curve (cm)	−0.3	−1.6	2.1	11.1
	height (m)	−7.9	−35.9	9.5	42.9
	volume (m^3)	−0.1	−28.3	0.2	47.3
FGI-HH-7	DBH (cm)	0.1	0.7	1.9	9.3
	stem curve (cm)	−0.1	−0.6	1.7	9.0
	height (m)	−6.4	−29.1	8.2	37.3
	volume (m^3)	−0.1	−24.9	0.2	44.4
FGI-HH-C	DBH (cm)	−1.3	−6.2	3.1	14.6
	stem curve (cm)	−1.6	−7.8	3.0	14.9
	height (m)	−1.0	−44.6	11.1	49.6
	volume (m^3)	−0.2	−38.8	0.3	55.5
HeliALS	DBH (cm)	−0.4	−1.7	4.2	16.7
	stem curve (cm)	0.5	2.4	4.5	20.0
	height (m)	-	-	-	-
	volume (m^3)	0.006	0.8	0.2	26.9

References

1. Kettunen, M.; Vihervaara, P.; Kinnunen, S.; D'Amato, D.; Badura, T.; Argimon, M.; Ten Brink, P. *Socio-Economic Importance of Ecosystem Services in the Nordic Countries*; Nordic Council of Ministers: Copenhagen, Denmark, 2012.
2. Luoma, V.; Saarinen, N.; Wulder, M.A.; White, J.C.; Vastaranta, M.; Holopainen, M.; Hyyppä, J. Assessing precision in conventional field measurements of individual tree attributes. *Forests* **2017**, *8*, 38. [CrossRef]
3. Wang, Y.; Lehtomäki, M.; Liang, X.; Pyörälä, J.; Kukko, A.; Jaakkola, A.; Liu, J.; Feng, Z.; Chen, R.; Hyyppä, J. Is field-measured tree height as reliable as believed—A comparison study of tree height estimates from field measurement, airborne laser scanning and terrestrial laser scanning in a boreal forest. *ISPRS J. Photogramm. Remote Sens.* **2019**, *147*, 132–145. [CrossRef]

4. Bragg, D.C. Accurately measuring the height of (real) forest trees. *J. For.* **2014**, *112*, 51–54. [CrossRef]
5. Bienert, A.; Scheller, S.; Keane, E.; Mohan, F.; Nugent, C. Tree detection and diameter estimations by analysis of forest terrestrial laserscanner point clouds. *Int. Arch. Photogramm. Remote Sens. Spat. Inf. Sci.* **2007**, *36*, 50–55.
6. Liang, X.; Kankare, V.; Yu, X.; Hyyppä, J.; Holopainen, M. Automated stem curve measurement using terrestrial laser scanning. *IEEE Trans. Geosci. Remote Sens.* **2014**, *52*, 1739–1748. [CrossRef]
7. Hyyppä, E.; Kukko, A.; Kaijaluoto, R.; White, J.C.; Wulder, M.A.; Pyörälä, J.; Liang, X.; Yu, X.; Wang, Y.; Kaartinen, H.; et al. Accurate derivation of stem curve and volume using backpack mobile laser scanning. *ISPRS J. Photogramm. Remote Sens.* **2020**, *161*, 246–262. [CrossRef]
8. Hyyppä, E.; Yu, X.; Kaartinen, H.; Hakala, T.; Kukko, A.; Vastaranta, M.; Hyyppä, J. Comparison of backpack, handheld, under-canopy UAV, and above-canopy UAV laser scanning for field reference data collection in boreal forests. *Remote Sens.* **2020**, *12*, 3327. [CrossRef]
9. Hyyppä, E.; Kukko, A.; Kaartinen, H.; Yu, X.; Muhojoki, J.; Hakala, T.; Hyyppä, J. Direct and automatic measurements of stem curve and volume using a high-resolution airborne laser scanning system. *Sci. Remote Sens.* **2022**, *5*, 100050. [CrossRef]
10. Liang, X.; Hyyppä, J.; Kaartinen, H.; Lehtomäki, M.; Pyörälä, J.; Pfeifer, N.; Holopainen, M.; Brolly, G.; Francesco, P.; Hackenberg, J.; et al. International benchmarking of terrestrial laser scanning approaches for forest inventories. *ISPRS J. Photogramm. Remote Sens.* **2018**, *144*, 137–179. [CrossRef]
11. de Paula Pires, R.; Olofsson, K.; Persson, H.J.; Lindberg, E.; Holmgren, J. Individual tree detection and estimation of stem attributes with mobile laser scanning along boreal forest roads. *ISPRS J. Photogramm. Remote Sens.* **2022**, *187*, 211–224. [CrossRef]
12. Laasasenaho, J. *Taper Curve and Volume Functions for Pine, Spruce and Birch*; Metsäntutkimuslaitos: Helsinki, Finland, 1982.
13. Bauwens, S.; Bartholomeus, H.; Calders, K.; Lejeune, P. Forest Inventory with Terrestrial LiDAR: A Comparison of Static and Hand-Held Mobile Laser Scanning. *Forests* **2016**, *7*, 127. [CrossRef]
14. Brede, B.; Lau, A.; Bartholomeus, H.; Kooistra, L. Comparing RIEGL RiCOPTER UAV LiDAR derived canopy height and DBH with terrestrial LiDAR. *Sensors* **2017**, *17*, 2371. [CrossRef] [PubMed]
15. Cabo, C.; Del Pozo, S.; Rodríguez-Gonzálvez, P.; Ordóñez, C.; González-Aguilera, D. Comparing terrestrial laser scanning (TLS) and wearable laser scanning (WLS) for individual tree modeling at plot level. *Remote Sens.* **2018**, *10*, 540. [CrossRef]
16. Gollob, C.; Ritter, T.; Nothdurft, A. Forest inventory with long range and high-speed personal laser scanning (PLS) and simultaneous localization and mapping (SLAM) technology. *Remote Sens.* **2020**, *12*, 1509. [CrossRef]
17. Oveland, I.; Hauglin, M.; Giannetti, F.; Schipper Kjørsvik, N.; Gobakken, T. Comparing three different ground based laser scanning methods for tree stem detection. *Remote Sens.* **2018**, *10*, 538. [CrossRef]
18. Liang, X.; Wang, Y.; Pyörälä, J.; Lehtomäki, M.; Yu, X.; Kaartinen, H.; Kukko, A.; Honkavaara, E.; Issaoui, A.E.; Nevalainen, O.; et al. Forest in situ observations using unmanned aerial vehicle as an alternative of terrestrial measurements. *For. Ecosyst.* **2019**, *6*, 20. [CrossRef]
19. Chudá, J.; Hunčaga, M.; Tucek, J.; Mokros, M. The handheld mobile laser scanners as a tool for accurate positioning under forest canopy. *ISPRS—Int. Arch. Photogramm. Remote Sens. Spat. Inf. Sci.* **2020**, *43*, 211–218. [CrossRef]
20. Tavi, D. Comparison of Under-Canopy Unmanned Aerial Vehicle, Airborne, and Ground-Based Mobile Laser Scanning for Forest Field Reference Measurements. Master's Thesis, Aalto University, Espoo, Finland, 2023.
21. Qian, C.; Liu, H.; Tang, J.; Chen, Y.; Kaartinen, H.; Kukko, A.; Zhu, L.; Liang, X.; Chen, L.; Hyyppä, J. An Integrated GNSS/INS/LiDAR-SLAM Positioning Method for Highly Accurate Forest Stem Mapping. *Remote Sens.* **2017**, *9*, 3. [CrossRef]
22. Tang, J.; Chen, Y.; Niu, X.; Wang, L.; Chen, L.; Liu, J.; Shi, C.; Hyyppä, J. LiDAR Scan Matching Aided Inertial Navigation System in GNSS-Denied Environments. *Sensors* **2015**, *15*, 16710–16728. [CrossRef]
23. Xie, Y.; Yang, T.; Wang, X.; Chen, X.; Pang, S.; Hu, J.; Wang, A.; Chen, L.; Shen, Z. Applying a Portable Backpack Lidar to Measure and Locate Trees in a Nature Forest Plot: Accuracy and Error Analyses. *Remote Sens.* **2022**, *14*, 1806. [CrossRef]
24. Kukko, A.; Kaijaluoto, R.; Kaartinen, H.; Lehtola, V.V.; Jaakkola, A.; Hyyppä, J. Graph SLAM correction for single scanner MLS forest data under boreal forest canopy. *ISPRS J. Photogramm. Remote Sens.* **2017**, *132*, 199–209. [CrossRef]
25. Proudman, A.; Ramezani, M.; Digumarti, S.T.; Chebrolu, N.; Fallon, M. Towards real-time forest inventory using handheld LiDAR. *Robot. Auton. Syst.* **2022**, *157*, 104240. [CrossRef]
26. Faitli, T.; Hakala, T.; Kaartinen, H.; Hyyppä, J.; Kukko, A. Real-time lidar-inertial positioning and mapping for forestry automation. *Int. Arch. Photogramm. Remote Sens. Spat. Inf. Sci.* **2023**, *48*, 145–150. [CrossRef]
27. Chen, S.; Liu, H.; Feng, Z.; Shen, C.; Chen, P. Applicability of personal laser scanning in forestry inventory. *PLoS ONE* **2019**, *14*, 1–22. [CrossRef] [PubMed]
28. Ryding, J.; Williams, E.; Smith, M.J.; Eichhorn, M.P. Assessing handheld mobile laser scanners for forest surveys. *Remote Sens.* **2015**, *7*, 1095–1111. [CrossRef]
29. Hyyppä, E.; Hyyppä, J.; Hakala, T.; Kukko, A.; Wulder, M.A.; White, J.C.; Pyörälä, J.; Yu, X.; Wang, Y.; Virtanen, J.P.; et al. Under-canopy UAV laser scanning for accurate forest field measurements. *ISPRS J. Photogramm. Remote Sens.* **2020**, *164*, 41–60. [CrossRef]
30. Hyyppä, J.; Yu, X.; Hakala, T.; Kaartinen, H.; Kukko, A.; Hyyti, H.; Muhojoki, J.; Hyyppä, E. Under-Canopy UAV Laser Scanning Providing Canopy Height and Stem Volume Accurately. *Forests* **2021**, *12*, 856. [CrossRef]

31. Liang, X.; Kukko, A.; Hyyppä, J.; Lehtomäki, M.; Pyörälä, J.; Yu, X.; Kaartinen, H.; Jaakkola, A.; Wang, Y. In-situ measurements from mobile platforms: An emerging approach to address the old challenges associated with forest inventories. *ISPRS J. Photogramm. Remote Sens.* **2018**, *143*, 97–107 . [CrossRef]
32. Giannetti, F.; Puletti, N.; Quatrini, V.; Travaglini, D.; Bottalico, F.; Corona, P.; Chirici, G. Integrating terrestrial and airborne laser scanning for the assessment of single-tree attributes in Mediterranean forest stands. *Eur. J. Remote Sens.* **2018**, *51*, 795–807. [CrossRef]
33. Jurjević, L.; Liang, X.; Gašparović, M.; Balenović, I. Is field-measured tree height as reliable as believed – Part II, A comparison study of tree height estimates from conventional field measurement and low-cost close-range remote sensing in a deciduous forest. *ISPRS J. Photogramm. Remote Sens.* **2020**, *169*, 227–241. [CrossRef]
34. Bienert, A.; Georgi, L.; Kunz, M.; Maas, H.G.; Von Oheimb, G. Comparison and Combination of Mobile and Terrestrial Laser Scanning for Natural Forest Inventories. *Forests* **2018**, *9*, 395. [CrossRef]
35. Kankare, V.; Vauhkonen, J.; Tanhuanpää, T.; Holopainen, M.; Vastaranta, M.; Joensuu, M.; Krooks, A.; Hyyppä, J.; Hyyppä, H.; Alho, P.; et al. Accuracy in estimation of timber assortments and stem distribution—A comparison of airborne and terrestrial laser scanning techniques. *ISPRS J. Photogramm. Remote Sens.* **2014**, *97*, 89–97. [CrossRef]
36. Kuželka, K.; Slavík, M.; Surovỳ, P. Very high density point clouds from UAV laser scanning for automatic tree stem detection and direct diameter measurement. *Remote Sens.* **2020**, *12*, 1236. [CrossRef]
37. Vandendaele, B.; Fournier, R.A.; Vepakomma, U.; Pelletier, G.; Lejeune, P.; Martin-Ducup, O. Estimation of northern hardwood forest inventory attributes using UAV laser scanning (ULS): Transferability of laser scanning methods and comparison of automated approaches at the tree-and stand-level. *Remote Sens.* **2021**, *13*, 2796. [CrossRef]
38. Wieser, M.; Mandlburger, G.; Hollaus, M.; Otepka, J.; Glira, P.; Pfeifer, N. A case study of UAS borne laser scanning for measurement of tree stem diameter. *Remote Sens.* **2017**, *9*, 1154. [CrossRef]
39. Puliti, S.; Breidenbach, J.; Astrup, R. Estimation of forest growing stock volume with UAV laser scanning data: Can it be done without field data? *Remote Sens.* **2020**, *12*, 1245. [CrossRef]
40. Liang, X.; Hyyppä, J.; Kaartinen, H.; Holopainen, M.; Melkas, T. Detecting changes in forest structure over time with bi-temporal terrestrial laser scanning data. *ISPRS Int. J. Geo-Inf.* **2012**, *1*, 242–255. [CrossRef]
41. Liang, X.; Hyyppä, J. Automatic stem mapping by merging several terrestrial laser scans at the feature and decision levels. *Sensors* **2013**, *13*, 1614–1634. [CrossRef] [PubMed]
42. Maas, H.G.; Bienert, A.; Scheller, S.; Keane, E. Automatic forest inventory parameter determination from terrestrial laser scanner data. *Int. J. Remote Sens.* **2008**, *29*, 1579–1593. [CrossRef]
43. Bazezew, M.N.; Hussin, Y.A.; Kloosterman, E. Integrating Airborne LiDAR and Terrestrial Laser Scanner forest parameters for accurate above-ground biomass/carbon estimation in Ayer Hitam tropical forest, Malaysia. *Int. J. Appl. Earth Obs. Geoinf.* **2018**, *73*, 638–652. [CrossRef]
44. Panagiotidis, D.; Abdollahnejad, A.; Slavik, M. 3D point cloud fusion from UAV and TLS to assess temperate managed forest structures. *Int. J. Appl. Earth Obs. Geoinf.* **2022**, *112*, 102917. [CrossRef]
45. Paris, C.; Kelbe, D.; Van Aardt, J.; Bruzzone, L. A novel automatic method for the fusion of ALS and TLS LiDAR data for robust assessment of tree crown structure. *IEEE Trans. Geosci. Remote Sens.* **2017**, *55*, 3679–3693. [CrossRef]
46. Shimizu, K.; Nishizono, T.; Kitahara, F.; Fukumoto, K.; Saito, H. Integrating terrestrial laser scanning and unmanned aerial vehicle photogrammetry to estimate individual tree attributes in managed coniferous forests in Japan. *Int. J. Appl. Earth Obs. Geoinf.* **2022**, *106*, 102658. [CrossRef]
47. Zhou, R.; Sun, H.; Ma, K.; Tang, J.; Chen, S.; Fu, L.; Liu, Q. Improving Estimation of Tree Parameters by Fusing ALS and TLS Point Cloud Data Based on Canopy Gap Shape Feature Points. *Drones* **2023**, *7*, 524. [CrossRef]
48. Wang, Y.; Kukko, A.; Hyyppä, E.; Hakala, T.; Pyörälä, J.; Lehtomäki, M.; El Issaoui, A.; Yu, X.; Kaartinen, H.; Liang, X.; et al. Seamless integration of above-and under-canopy unmanned aerial vehicle laser scanning for forest investigation. *For. Ecosyst.* **2021**, *8*, 10. [CrossRef]
49. Kankare, V.; Liang, X.; Vastaranta, M.; Yu, X.; Holopainen, M.; Hyyppä, J. Diameter distribution estimation with laser scanning based multisource single tree inventory. *ISPRS J. Photogramm. Remote Sens.* **2015**, *108*, 161–171. [CrossRef]
50. Wang, Y.; Pyörälä, J.; Liang, X.; Lehtomäki, M.; Kukko, A.; Yu, X.; Kaartinen, H.; Hyyppä, J. In situ biomass estimation at tree and plot levels: What did data record and what did algorithms derive from terrestrial and aerial point clouds in boreal forest. *Remote Sens. Environ.* **2019**, *232*, 111309. [CrossRef]
51. SCAN FOREST. Scan Forest Research Infrastructure Website. 2024. Available online: https://www.scanforest.fi (accessed on 20 March 2024).
52. Velodyne Lidar. VLP-16 User Manual. 2019. 63-9243 Rev. E. Available online: https://velodynelidar.com/wp-content/uploads/2019/12/63-9243-Rev-E-VLP-16-User-Manual.pdf (accessed on 3 January 2024).
53. Ouster. Ouster OS0 Rev. 5 Datasheet. 2021. Available online: https://data.ouster.io/downloads/datasheets/datasheet-rev05-v2p1-os0.pdf (accessed on 24 August 2021).
54. Ouster. Ouster OS0 Rev. C Datasheet. 2023. Available online: https://data.ouster.io/downloads/datasheets/datasheet-revc-v2p5-os0.pdf (accessed on 4 May 2023).
55. Ouster. Ouster OS0 Rev. 7 Datasheet. 2023. Available online: https://data.ouster.io/downloads/datasheets/datasheet-rev7-v3p0-os0.pdf (accessed on 4 May 2023).

56. RIEGL. VUX-1HA Datasheet. 2023. Available online: http://www.riegl.com/uploads/tx_pxpriegldownloads/RIEGL_VUX-1HA-22_Datasheet_2023-04-25.pdf (accessed on 2 March 2024).
57. Leica Geosystems. Leica RTC360 Datasheet. 2018. Available online: https://leica-geosystems.com/-/media/files/leicageosystems/products/datasheets/leica-rtc360-ds-872750-0821-en.ashx?la=da&hash=30083BF63CCCE6919BD7964EEC5ADC77 (accessed on 2 January 2024).
58. Hyyppä, J.; Inkinen, M. Detecting and estimating attributes for single trees using laser scanning. *Photogramm. J. Finl.* **1999**, *16*, 27–42.
59. Næsset, E.; Gobakken, T.; Holmgren, J.; Hyyppä, H.; Hyyppä, J.; Maltamo, M.; Nilsson, M.; Olsson, H.; Persson, Å.; Söderman, U. Laser scanning of forest resources: The Nordic experience. *Scand. J. For. Res.* **2004**, *19*, 482–499. [CrossRef]
60. Hyyppä, E.; Muhojoki, J.; Yu, X.; Kukko, A.; Kaartinen, H.; Hyyppä, J. Efficient coarse registration method using translation-and rotation-invariant local descriptors towards fully automated forest inventory. *ISPRS Open J. Photogramm. Remote Sens.* **2021**, *2*, 100007. [CrossRef]
61. Meyer, F. Topographic distance and watershed lines. *Signal Process.* **1994**, *38*, 113–125. [CrossRef]
62. Ester, M.; Kriegel, H.P.; Sander, J.; Xu, X. A density-based algorithm for discovering clusters in large spatial databases with noise. In Proceedings of the Second International Conference on Knowledge Discovery and Data Mining, Portland, OR, USA, 2–4 August 1996; pp. 226–231.
63. Fischler, M.A.; Bolles, R.C. Random sample consensus: A paradigm for model fitting with applications to image analysis and automated cartography. *Commun. ACM* **1981**, *24*, 381–395. [CrossRef]
64. Forsman, M.; Börlin, N.; Olofsson, K.; Reese, H.; Holmgren, J. Bias of cylinder diameter estimation from ground-based laser scanners with different beam widths: A simulation study. *ISPRS J. Photogramm. Remote Sens.* **2018**, *135*, 84–92. [CrossRef]
65. Muhojoki, J.; Hakala, T.; Kukko, A.; Kaartinen, H.; Hyyppä, J. Comparing positioning accuracy of mobile laser scanning systems under a forest canopy. *Sci. Remote Sens.* **2024**, *9*, 100121. [CrossRef]
66. Ringdahl, O.; Hohnloser, P.; Hellström, T.; Holmgren, J.; Lindroos, O. Enhanced Algorithms for Estimating Tree Trunk Diameter Using 2D Laser Scanner. *Remote Sens.* **2013**, *5*, 4839–4856. [CrossRef]
67. Kuželka, K.; Surový, P. Noise Analysis for Unbiased Tree Diameter Estimation from Personal Laser Scanning Data. *Remote Sens.* **2024**, *16*, 1261. [CrossRef]
68. Hyyppä, J.; Mielonen, T.; Hyyppä, H.; Maltamo, M.; Yu, X.; Honkavaara, E.; Kaartinen, H. Using individual tree crown approach for forest volume extraction with aerial images and laser point clouds. In Proceedings of the ISPRS Workshop Laser Scanning, Enschede, The Netherlands, 12–15 September 2005, pp. 144–149.
69. Xi, Z.; Hopkinson, C. 3D Graph-Based Individual-Tree Isolation (Treeiso) from Terrestrial Laser Scanning Point Clouds. *Remote Sens.* **2022**, *14*, 6116. [CrossRef]
70. Soininen, V.; Hyyppä, E.; Muhojoki, J.; Luoma, V.; Kaartinen, H.; Lehtomäki, M.; Kukko, A.; Hyyppä, J. Accuracy comparison of terrestrial and airborne laser scanning and manual measurements for stem curve-based growth measurements of individual trees. *Sci. Remote Sens.* **2024**, *9*, 100125. [CrossRef]